Proceedings of ISERME 2025
19-20 September 2025
https://doi.org/10.31705/ISERME.2025.7

Deformation Monitoring of Tailings Storage Facilities Using InSAR Time Series on OpenSARLab

***Sanchez[1] V, Cabrera[2] F, Okada[3] N, Ohtomo[3] Y, Suorineni[4] F, and Kawamura[4] Y**

[1]Division of Sustainable Resources Engineering, Graduate School of Engineering, Hokkaido University, Sapporo, Japan

[2]UTE University, Faculty of Architecture and Urbanism, Architecture Department, LL Liminal Lab Research Group, 170527, Quito, Ecuador

[3]Division of Sustainable Resources Engineering, Faculty of Engineering, Hokkaido University, Sapporo, Japan

[4]School of Mining and Geosciences, Department of Mining Engineering, Nazarbayev University, 53 Kabanbay Batyr Avenue, Astana, Kazakhstan

*Corresponding author – yvane18sanchez@gmail.com

Abstract

Tailings storage facilities (TSFs) are essential components of mining operations, designed to contain byproducts from mineral processing. However, their structural failure can lead to catastrophic environmental damage, loss of life, and long-term socioeconomic disruption. Continuous, high-resolution monitoring is therefore vital for early detection of instability and informed risk management. In this study, 161 ascending Sentinel-1 acquisitions were processed using the SBAS-InSAR technique within OpenSARLab, a cloud-based platform that enables scalable, reproducible analysis of satellite radar data. Despite challenges posed by dense tropical vegetation and frequent rainfall, applying a coherence threshold of 0.6 yielded broad spatial coverage, with a mean coherence of 0.70 across 249 observation points. This allowed for reliable displacement retrieval even in vegetated zones. Mean LOS velocities ranged from −7.46 to +2.83 cm/yr, with 94% of the area showing subsidence. The embankment crest was the most mobile, averaging −4.67 cm/yr, with cumulative deformation reaching −0.42 m in the west sector by 2025. Time-series analysis revealed stepwise accelerations coinciding with heavy rainfall events (≥150–250 mm/month), suggesting rainfall-modulated creep rather than imminent failure. To improve early-warning capabilities, future work should integrate GNSS control points and detailed construction records to calibrate thresholds and strengthen causal interpretation.

Keywords: OpenSARLab, SBAS InSAR, Tailings dam stability, Tropical environments

1 Introduction

The global demand for metals, driven by technological innovation, infrastructure development, and energy transition, has led to increased mining activity and a growing number of tailings storage facilities (TSFs) [1]. Tailings, the fine residues from mineral processing, are commonly deposited as slurry in engineered dams [2]. TSF failures, with a global rate of ~1.2%, far higher than the 0.01% failure rate of conventional water dams, poses severe environmental, social, and economic risks [3], [4]. Their safe management requires continuous monitoring across the entire lifecycle. While inspections and in-situ instrumentation remain essential, their limitations in coverage and cost have motivated the use of satellite remote sensing, which offers wide-area, frequent, and cost-effective monitoring [5].

Interferometric Synthetic Aperture Radar (InSAR) is a remote sensing technique capable of detecting ground deformation with millimeter accuracy through repeated SAR acquisitions [6].

Multi-temporal InSAR (MT-InSAR) approaches, such as the Small Baseline Subset (SBAS) method [7], address the wavelength and coherence limitations of single interferograms by integrating long time-series of short-baseline pairs [8]. A key step in this process is evaluating coherence values to filter out noisy pixels [9], ensuring a reliable dataset for deformation analysis.

Building on this, SBAS-InSAR is particularly advantageous in vegetated environments, where temporal and geometric decorrelation often reduce signal quality. By enhancing phase stability, SBAS allows consistent displacement estimates from distributed scatterers [10], [11], and has been successfully applied to landslide monitoring, subsidence detection, and infrastructure assessment [12]. However, applying SBAS to large datasets and long time series is computationally intensive, requiring significant storage and processing capacity.

To overcome these challenges, cloud-based platforms such as OpenSARLab, developed by the University of Alaska Fairbanks, provide a JupyterHub environment with pre-installed SAR tools for advanced InSAR analysis without the need for local resources [13]. In collaboration with NASA, the Alaska Satellite Facility (ASF) also offers On-Demand processing via Vertex, generating Sentinel-1 interferometric products at 40 m or 80 m resolution [14]. While OpenSARLab has been extensively applied in landslide research, its use in TSF monitoring remains limited, with only a few studies exploring this field.

This study uses SBAS-InSAR via OpenSARLab to analyze deformation at an active TSF in a tropical region of South America. The site stores tailings from a gold processing plant, spanning approximately 0.25 km^2. A time-series was derived from 161 ascending Sentinel-1 scenes (Jan 2020–Jul 2025), revealing deformation concentrated on the crest of the main embankment, while surrounding vegetated zones showed stable displacement and good coherence. LOS displacement trends were compared with daily rainfall data to evaluate precipitation-related impacts on embankment stability.

2 Methodology

Sentinel-1 Level-1 Single Look Complex (SLC) images in Interferometric Wide (IW) mode were processed using the ASF HyP3 platform, which employs GAMMA software up to the phase unwrapping stage. The study used 161 Sentinel-1 ascending acquisitions in track 18, covering 54 months. To build the interferometric network, the SBAS criteria were applied, retaining pairs with perpendicular baselines shorter than 200 m and temporal baselines of 12 days. This filtering minimized decorrelation and preserved coherence in vegetated areas, resulting in a stack of 149 unwrapped interferograms.

The time-series analysis was performed in the OpenSARLab cloud environment using MintPy InSAR Time-Series software in Jupyter notebooks (https://github.com/insarlab/MintPy) [15]. This framework implements the SBAS approach, taking as input the HyP3 interferograms stack, which already have topographic correction applied by GAMMA software using SRTM DEM (Shuttle Radar Topography Mission).

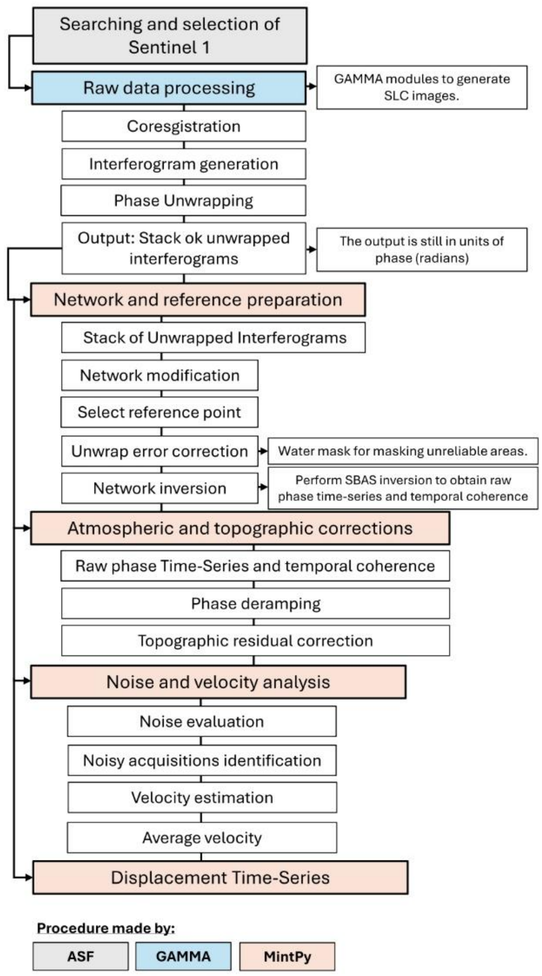

Figure 1: Workflow of the methodology applied, illustrating the MintPy processing steps executed within the OpenSARLab platform.

Within the processing workflow, the interferogram stack is first geocoded to align spatially with the study area. The phase information is then extracted and refined through multiple correction steps aimed at minimizing noise unrelated to actual ground movement. Once the corrections are validated, the cleaned phase data is translated into deformation time series and mean line-of-sight (LOS) velocity maps, which serve as the basis for calculating the total magnitude of surface displacement. The workflow (Figure 1) enables efficient end-to-end processing without the need for local storage or software installations.

3 Results

The following LOS displacement results are from 249 observation points (OP) that are spread on surrounding vegetated area (V), access roads to the TSF (R), infrastructure (I), tailings pond (T), and embankment (E/B), further divided into toe (E/B T) and crest (E/B C).

To ensure reliable deformation estimates, pixels with low signal quality were filtered using a coherence threshold of **0.6.** Table 1 summarizes the average coherence in seven different sectors.

Table 2: Mean values of coherence, velocity and observation points by sector.

Sector	Mean coherence	Mean velocity [cm/yr]	OP
V	0.69	-0.96	69
R	0.69	-0.94	35
I	0.74	-0.55	23
T	0.68	-2.93	43
E/B	0.71	-3.58	66
E/B T	0.79	-0.99	5
E/B C	0.71	-4.67	8

Coherence values across the study area range from 0.68 to 0.79 with a mean of 0.70.

Analysis of the results revealed mean LOS velocities range from –7.46 to +2.83 cm/yr, with approximately 94% of the area showing subsidence, most pronounced is the main embankment central western area as depicted in Figure 2.

From Table 1 LOS deformation velocities can be analyzed. The vegetated surroundings (V), access roads (R), and infrastructure (I) remain stable, with mean velocities between –0.55 and –0.96 cm/yr. The tailings pond (T) shows greater subsidence (–2.93 cm/yr), However, the embankment records the most significant movements: the main body (E/B) at –3.58 cm/yr, the toe (E/B T) at –0.99 cm/yr, and the crest (E/B C) with the highest rate (–4.67 cm/yr).

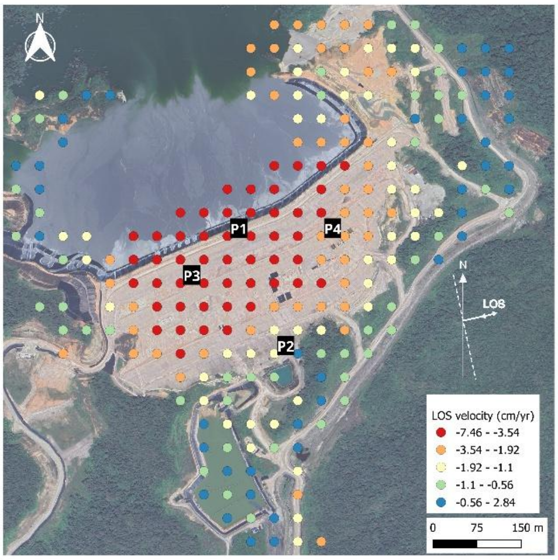

Figure 2: Illustration of InSAR velocity measurements over the case study averaged over the whole SAR data stack. Basemap image copyright ©Google Earth.

To assess fluctuations in displacement trends, one point with the highest LOS displacement was selected from each sector. Figure 3 illustrates the displacement patterns for these points, highlighting five distinct acceleration periods. During these intervals, velocities ranged from –4.0 to –37.0 cm/yr. The highest acceleration rates were recorded at points located directly on the dam, reaching 37.17 cm/yr in 2022.

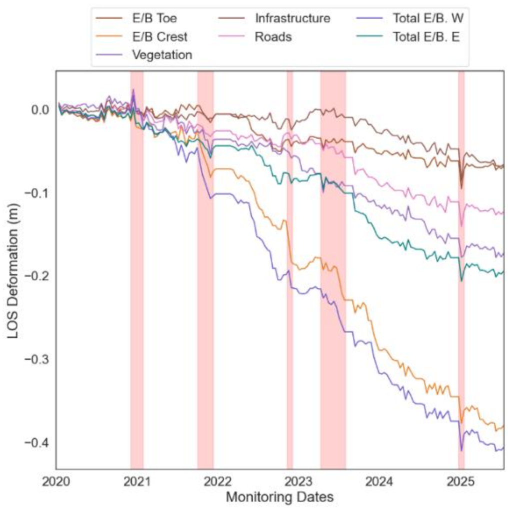

Figure 3: Time-series LOS displacements and acceleration periods by sector.

On the other hand, previous InSAR studies have shown strong potential for detecting erosion linked to intense precipitation [16]. With C-band sensitivity, InSAR captures millimeter-scale elevation changes from surface water movement [17]. In this analysis, rainfall data was used to evaluate whether high-precipitation phases coincide with displacement spikes.

Figure 4 displays LOS time-series displacements at four representative points along the TSF embankment, located on the crest, the west and east sectors, and the toe, spatially referenced in Figure 1. Since early 2022, following several months with rainfall totals between 150–250 mm, the embankment has exhibited stepwise subsidence modulated by precipitation intensity. By 2025, cumulative displacements reached approximately −0.42 m in the west sector, −0.37 m on the crest, −0.21 m in the east sector, and −0.12 m at the toe.

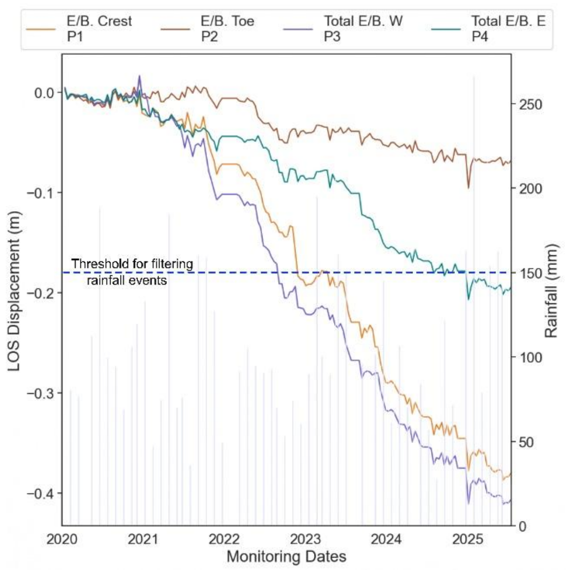

Figure 4: Time-series LOS displacements for embankment points P1, P2, P3, and P4, overlaid with monthly rainfall records.

4 Discussion

Coherence values across the study area range from 0.68 to 0.79, indicating reliable interferometric quality for SBAS-InSAR analysis. Despite surrounding vegetation, several zones maintain coherence above 0.69, enabling meaningful displacement monitoring. Areas like I and R, though non-vegetated, show strong point density, supporting deformation tracking in unstructured terrain. The embankment infrastructure exhibits consistently high coherence (>0.75), reflecting engineered surfaces that enhance radar return and ensure robust coverage, underscoring the importance of targeted point selection and coherence filtering in tropical, vegetated settings.

The tailings pond exhibits notable subsidence (–2.93 cm/yr), consistent with the progressive consolidation of fine-grained tailings material in its beach. This rate was derived from MT-DInSAR LOS displacement time series, with a standard deviation of ±0.4 cm/yr [18], reflecting stable coherence and consistent phase unwrapping across the monitored period. The embankment shows the most significant deformation, reflecting a common characteristic of tailings dam design, where construction phases often overlap with operational activity. This overlap, observed throughout the facility's lifespan [19] contributes to recurrent variability in the time-series displacement.

Fluctuations in displacement trends should be analyzed in conjunction with the embankment construction schedule to assess potential correlations between observed acceleration rates and dynamic conditions during dam raising. The highest acceleration, 37.17 cm/year, was recorded at monitoring points situated directly on the dam, indicating that the construction process may introduce noise into deformation measurements. However, due to limited access to detailed construction timelines, these elevated acceleration rates cannot yet be conclusively interpreted as indicators of impending structural failure.

While construction-related acceleration remains inconclusive, rainfall emerges as a likely driver of dam mobility. In this study, daily rainfall data were obtained from the nearest meteorological station operated by the local government. To align with the 12-day acquisition interval of the Sentinel-1 MT-DInSAR time series, precipitation values were aggregated over each corresponding period to enable comparative analysis with LOS deformation trends. This temporal alignment allowed for a focused investigation into the relationship between rainfall intensity and deformation behavior. Specifically, the analysis aimed to determine whether high-precipitation phases coincide with displacement spikes. Table 2 presents filtered events (≥150 mm), where some points on the embankment exhibit stepwise, rainfall-modulated subsidence that stabilizes between storms, suggesting rainfall-driven behavior rather than pre-failure acceleration. West point is most sensitive (6 responses; largest −3.59 cm, ~12-day lag), followed by Crest (4), Toe (4), and

East (3). All flagged responses occur at a modal lag of 12 days, consistent with the InSAR revisit interval; however, the true physical lag could be ≤12 days (likely hours–days).

Table 2: Influence of rainfall events on InSAR Displacement Response

Point	Rain date	Rain [mm]	Displ. [cm]
E/B C	10/11/2021	158.7	-1.31
E/B C	7/3/2023	151	-1.64
E/B C	4/16/2024	161.1	-1.56
E/B C	12/24/2024	162.6	-3.23
E/B T	10/11/2021	158.7	-0.71
E/B T	4/16/2024	161.1	-0.74
E/B T	5/10/2024	210.7	-0.84
E/B T	12/24/2024	162.6	-3.36
E/B W	6/13/2021	197.8	-0.96
E/B W	10/11/2021	158.7	-1.65
E/B W	7/3/2023	151	-0.84
E/B W	4/16/2024	161.1	-1.56
E/B W	5/10/2024	210.7	-0.64
E/B W	12/24/2024	162.6	-3.59
E/B E	4/16/2024	161.1	-0.92
E/B E	5/10/2024	210.7	-0.92
E/B E	12/24/2024	162.6	-2.85

5 Conclusions

After coherence filtering at 0.6, mean coherence across observation points is 0.70 (embankment >0.75), enabling reliable SBAS-InSAR deformation retrieval even over surrounding vegetation (several observation points ≥0.69).

Displacement analysis indicates pervasive subsidence (94% of the area), with the embankment hosting the largest deformations, both in rate and magnitude: the crest averages −4.67 cm/yr LOS velocity. The time series shows five acceleration phases, peaking at 37.17 cm/yr in 2022. While construction-related triggers remain unverified due to limited raising schedules, rainfall is the dominant control: step-like subsidence follows months with ≥150 mm precipitation, with the west sector showing the strongest response, consistent with spatial contrasts in drainage capacity and/or material properties.

Although MT-InSAR deformations trends in this case study could be explained using rainfall records, key limitations are the absence of GNSS and detailed construction schedules, which currently preclude rigorous calibration and attribution. However, such reference data is often unavailable. Despite this limitation, previous studies have successfully revealed ground deformation precursors to the Brumadinho Tailings Dam collapse, which is surrounded by vegetated areas [19], [20], [21].

Future work will improve deformation monitoring by co-locating GNSS points on key embankment sectors to validate InSAR velocities. Incorporating construction phase records will clarify whether displacement trends reflect operational activity or structural response. Once validated, rainfall-displacement correlations will be used to define velocity thresholds and support early-warning protocols suited to tropical, high-rainfall settings.

MT-DInSAR should be considered a complementary tool within mine safety management systems, rather than a standalone solution. While real-time instrumentation remains essential for operational decision-making, satellite-based deformation monitoring provides valuable retrospective insights. It has proven capable of detecting subtle accelerations prior to failure events, offering an additional layer of spatial context and early warning potential for regulatory oversight and risk mitigation.

Acknowledgements

The researchers express their gratitude to SATREPS, JST, and JICA for their invaluable support of the Japan-Kazakhstan SATREPS Knight Project throughout this study.

References

[1] M. Zare, F. Nasategay, J. A. Gomez, A. Moayedi Far, and J. Sattarvand, “A Review of Tailings Dam Safety Monitoring Guidelines and Systems,” *Minerals*, vol. 14, no. 6, p. 551, May 2024, doi: 10.3390/min14060551.

[2] M. G. Sottile, N. A. Labanda, A. Kerguelén, I. A. Cueto, and A. O. Sfriso, “Stability Assessment of a Tailings Storage Facility Using a Non-local Constitutive Model Accounting for Anisotropic Strain-Softening,” 2021, pp. 334–342. doi: 10.1007/978-3-030-64518-2_40.

[3] . J. Williams, “Lessons from Tailings Dam Failures—Where to Go from Here?,”*Minerals*, vol. 11, no. 8, p. 853, Aug. 2021, doi: 10.3390/min11080853.

[4] T. Hao, X. Zheng, H. Wang, K. Xu, and Y. Yu, “Development of a method for weight

determination of disaster-causing factors and quantitative risk assessment for tailings dams based on causal coupling relationships," *Stochastic Environmental Research and Risk Assessment*, vol. 37, no. 2, pp. 749–775, Feb. 2023, doi: 10.1007/s00477-022-02316-w.

[5] P. B. McKenna, A. M. Lechner, S. Phinn, and P. D. Erskine, "Remote Sensing of Mine Site Rehabilitation for Ecological Outcomes: A Global Systematic Review," *Remote Sens (Basel)*, vol. 12, no. 21, p. 3535, Oct. 2020, doi: 10.3390/rs12213535.

[6] R. F. Hanssen, "Stochastic model for radar interferometry," in *Radar Interferometry*, 2001, pp. 81–159. doi: 10.1007/0-306-47633-9_4.

[7] P. Berardino *et al.*, "Small baseline DINSAR techniques for earth surface deformation analysis," in *Third International Workshop on ERS SAR Interferometry "FRINCE03,"* 2003.

[8] T. Wang, M. Liao, and D. Perissin, "InSAR coherence-decomposition analysis," *IEEE Geoscience and Remote Sensing Letters*, vol. 7, no. 1, pp. 156–160, Sep. 2009.

[9] T. Wang, M. Liao, and D. Perissin, "InSAR Coherence-Decomposition Analysis," *IEEE Geoscience and Remote Sensing Letters*, vol. 7, no. 1, pp. 156–160, Jan. 2010, doi: 10.1109/LGRS.2009.2029126.

[10] A. Hooper, D. Bekaert, K. Spaans, and M. Arıkan, "Recent advances in SAR interferometry time series analysis for measuring crustal deformation," *Tectonophysics*, vol. 514–517, pp. 1–13, Jan. 2012, doi: 10.1016/j.tecto.2011.10.013.

[11] A. Ferretti, C. Prati, and F. Rocca, "Permanent scatterers in SAR interferometry," *IEEE Transactions on Geoscience and Remote Sensing*, vol. 39, no. 1, pp. 8–20, 2001, doi: 10.1109/36.898661.

[12] P. Berardino *et al.*, "A quantitative analysis of the SBAS algorithm performance," in *IEEE International IEEE International IEEE International Geoscience and Remote Sensing Symposium, 2004. IGARSS '04. Proceedings. 2004*, IEEE, 2004, pp. 3321–3324. doi: 10.1109/IGARSS.2004.1370414.

[13] F. J. Meyer, P. A. Rosen, A. Flores, E. R. Anderson, and E. A. Cherrington, "Making Sar Accessible: Education & Training in Preparation for Nisar," in *2021 IEEE International Geoscience and Remote Sensing Symposium IGARSS*, IEEE, Jul. 2021, pp. 6–9. doi: 10.1109/IGARSS47720.2021.9554822.

[14] S. R. Chowdhury, D. S. Vaka, Y. S. Rao, and A. Bhattacharya, "Landslide Deformation Analysis Over Joshimath Region Using The Opensarlab Cloud-Based Environment," in *2024 IEEE India Geoscience and Remote Sensing Symposium (InGARSS)*, IEEE, Dec. 2024, pp. 1–4. doi: 10.1109/InGARSS61818.2024.10984126.

[15] Z. Yunjun, H. Fattahi, and F. Amelung, "Small baseline InSAR time series analysis: Unwrapping error correction and noise reduction," *Comput Geosci*, vol. 133, p. 104331, Dec. 2019, doi: 10.1016/j.cageo.2019.104331.

[16] W. R. Neely, A. A. Borsa, J. A. Burney, M. C. Levy, F. Silverii, and M. Sneed, "Characterization of Groundwater Recharge and Flow in California's San Joaquin Valley From InSAR-Observed Surface Deformation," *Water Resour Res*, vol. 57, no. 4, Apr. 2021, doi: 10.1029/2020WR028451.

[17] C. Nuncio, "Geophysical Delineation of Sandstone-Hosted Uranium Deposits in Shirley Basin," Master, University of Wyoming, Laramie USA, 2025.

[18] F. Cigna, R. Esquivel Ramírez, and D. Tapete, "Accuracy of Sentinel-1 PSI and SBAS InSAR Displacement Velocities against GNSS and Geodetic Leveling Monitoring Data," *Remote Sens (Basel)*, vol. 13, no. 23, p. 4800, Nov. 2021, doi: 10.3390/rs13234800.

[19] Y. Yan, H. Yu, and Y. Wang, "Alarming a tailings dam failure with a joint analysis of InSAR-derived surface deformation and SAR-derived moisture content," *Remote Sens Environ*, vol. 300, p. 113910, Jan. 2024, doi: 10.1016/j.rse.2023.113910.

[20] S. Das, A. Priyadarshana, and S. Grebby, "Monitoring the risk of a tailings dam collapse through spectral analysis of satellite InSAR time-series data," *Stochastic Environmental Research and Risk Assessment*, vol. 38, no. 8, pp. 2911–2926, Aug. 2024, doi: 10.1007/s00477-024-02713-3.

[21] L. H. Silva Rotta *et al.*, "The 2019 Brumadinho tailings dam collapse: Possible cause and impacts of the worst human and environmental disaster in Brazil," *International Journal of Applied Earth Observation and Geoinformation*, vol. 90, p. 102119, Aug. 2020, doi: 10.1016/j.jag.2020.102119.